Nanoparticle Brownian motion and hydrodynamic interactions in the presence of flow fields

B. Uma,[1,2,3] T. N. Swaminathan,[1,2] R. Radhakrishnan,[3] D. M. Eckmann,[2,3] and P. S. Ayyaswamy[1,a)]
[1]*Department of Mechanical Engineering and Applied Mechanics, University of Pennsylvania, Philadelphia, Pennsylvania 19104, USA*
[2]*Department of Anesthesiology and Critical Care, University of Pennsylvania, Philadelphia, Pennsylvania 19104, USA*
[3]*Department of Bioengineering, University of Pennsylvania, Philadelphia, Pennsylvania 19104, USA*

(Received 16 December 2010; accepted 27 June 2011; published online 26 July 2011)

We consider the Brownian motion of a nanoparticle in an incompressible Newtonian fluid medium (quiescent or fully developed Poiseuille flow) with the fluctuating hydrodynamics approach. The formalism considers situations where both the Brownian motion and the hydrodynamic interactions are important. The flow results have been modified to account for compressibility effects. Different nanoparticle sizes and nearly neutrally buoyant particle densities are also considered. Tracked particles are initially located at various distances from the bounding wall to delineate wall effects. The results for thermal equilibrium are validated by comparing the predictions for the temperatures of the particle with those obtained from the equipartition theorem. The nature of the hydrodynamic interactions is verified by comparing the velocity autocorrelation functions and mean square displacements with analytical and experimental results where available. The equipartition theorem for a Brownian particle in Poiseuille flow is verified for a range of low Reynolds numbers. Numerical predictions of wall interactions with the particle in terms of particle diffusivities are consistent with results, where available. © *2011 American Institute of Physics*. [doi:10.1063/1.3611026]

I. INTRODUCTION

A significant aspect of modeling nanoparticle motion in an incompressible fluid is the accurate evaluation of the associated momentum transport with or without bulk fluid flow. The modeling should account both for the Brownian motion and the hydrodynamic interactions and resolve the translational and rotational motions that arise. Effects of particle locations in the flow domain and of the presence of the wall must be delineated. The effects on particle diffusivity must be resolved.

The theory of non-equilibrium statistical mechanics indicates that the influence of thermal fluctuations on a mechanical system can typically be represented through the addition of thermal forcing terms to the equations governing the system. The thermal forcing terms following the statistics of a white nose rapidly decorrelate in time. The related hydrodynamics, however, involves a non-trivial structure of correlations between the state variables. In order to achieve thermal equilibrium, the correlations should be such that there is an energy balance between the thermal forcing and the dissipation of the system as required by the fluctuation-dissipation theorem.[1,2]

In Brownian simulations, there exist two different approaches to couple the thermal fluctuations with the hydrodynamic interactions. These are Langevin approach[3] and fluctuating hydrodynamics approach.[4] In the present study, we adopt the fluctuating hydrodynamics approach. This essentially consists of adding stochastic stresses to the stress tensor (random stress) and stochastic fluxes to the heat flux (where an energy equation is present in the formulation).[5]

Over the past decades, numerical simulations of the fluctuating hydrodynamics approach have been carried out employing the finite volume method,[6,7] lattice Boltzmann method (LBM),[8–14] and stochastic immersed boundary method.[15] A coarse-graining methodology has been developed to bridge molecular dynamics and fluctuating hydrodynamic simulations.[16,17] Serrano and Español[18] and Serrano *et al.*[19] have solved the fluctuating hydrodynamic Navier-Stokes equations without a particle using the finite volume Lagrangian discretization in a moving Voronoi grid. They have ensured that their discretized governing equations cast in the general equation for non-equilibrium reversible/irreversible coupling (GENERIC) formalism[20,21] satisfies the fluctuation-dissipation theorem. The GENERIC formalism proposed by Grmela and Öttinger[20] and Öttinger and Grmela[21] ensures the correct treatment of thermal fluctuations and fluctuating hydrodynamics. Patankar has simulated the thermal motion of two dimensional particles in a stationary medium with the finite element method (FEM).[11] Sharma and Patankar[6] have employed a distributed-Lagrangian multiplier (DLM) based finite volume method to simulate the thermal motion of particles. The computational domain is periodic in all directions and the thermal fluctuations are included in the fluid equations using random stress tensor. They have validated the numerical results by comparison with analytical expressions. Nie and Lin[14] have employed the fluctuating LBM to simulate Brownian motion of particles and have validated their numerically obtained velocity autocorrelation function (VACF) by comparison with theoretical predictions. It is shown that the

a)Author to whom correspondence should be addressed. Electronic mail: ayya@seas.upenn.edu.

temperature characterizing translational motion of the particle in three coordinate directions agrees with each other after a lapse of time, but the predicted particle temperature is 15% lower than the effective temperature of the fluid fluctuations. This is in accord with the earlier findings of Ladd,[10] who first proposed the use of fluctuating LBM. Adhikari *et al.*[12] have established agreement between fluctuation and dissipation by introducing ghost noise to the fluctuating LBM in the formulation (see Dünweg and Ladd[13] for further discussions of Ref. 12).

In this paper, we employ a direct numerical simulation (DNS) based on arbitrary Lagrangian-Eulerian (ALE) FEM (Refs. 22–25) to accurately resolve the complicated fluid-particle interfacial motions. Both translational and rotational motions of a nanoparticle in a (i) stationary fluid medium and (ii) Poiseuille flow are investigated. Heat flux (energy equation) is not considered. An unstructured finite element mesh, generated by the Delaunay-Voronoi method,[26] has enabled a significantly higher number of mesh points in the regions of interest (*i.e.*, close to the particle and wall surfaces compared to the regions farther away). This feature also keeps the overall mesh size computationally reasonable even with a nanoparticle moving in a very large domain.[22,23,27–29] Thermal fluctuations are included in the equations of linearized hydrodynamics by adding stochastic components to the stress tensor as white noise in space and time.[4,30] As noted in Español *et al.*,[30] "even though the original equations of fluctuating hydrodynamics are written in terms of stochastic partial differential equations, at a very fundamental level, the inclusion of thermal fluctuations requires always the notion of a "mesoscopic cell" in order to define the fluctuating quantities." In Español *et al.*,[30] it is shown that fluctuating hydrodynamic equations discretized in terms of finite element shape functions based on the Delaunay triangulation satisfy the fluctuation-dissipation theorem. The numerical schemes for the implementation of thermal fluctuations in the Landau-Lifshitz Navier-Stokes equations are expected to perform very delicate tasks[31,32] and obtaining accurate numerical results is a challenging endeavor.

It has been extensively discussed in the literature that the relation between fluctuation and dissipation is impacted by the compressibility of the fluid.[33–36] However, our objective is to keep the numerical model within the frame work of an incompressible liquid assumption. To account for compressibility, following Zwanzig and Bixon,[34] we modify the numerically predicted results to take into account the energy carried by sound waves. For real liquids of technological interest, such as water, blood *etc.*, a numerical route to simulate the hydrodynamics is only practical by invoking this feature. With a finite element model, the accounting for the compressibility in the liquid medium would be very complicated, even if we knew the highly non-trivial equation of state. Furthermore, the approach employed in this paper is easily extendable to several biological applications.[37,38]

The chief motivation for the present study is the simulation of a nanoparticle thermal motion in a fluid flow that occurs in targeted drug delivery (TDD) and microparticle flows, such as the motion of a particle through a nanochannel.[39,40] In TDD, the drug carrying nanocarriers are intravascularly introduced into the vasculature.[41–43] The drug-laden nanocarriers are functionalized with ligands (*e.g.*, antibodies) and recognize specific determinants (receptors) expressed by endothelial cells.[38,44] The receptor-ligand binding interactions at the involved sites define the efficacy of nanocarrier arrest by the targeted cell. Since the drug-laden nanocarrier, essentially neutrally buoyant, is delivered to a therapeutic target via the vasculature, its motion in a bloodstream has to be determined accurately. In order to achieve this goal, as a first step, it is necessary to determine the motion of a nanocarrier (due to thermal and hydrodynamic effects) in an incompressible Newtonian fluid. The numerical methodology developed in this study is aimed at that objective.

The paper is organized as follows. Section II describes the mathematical formulation of the problem. Section III explains the Galerkin finite element formulation of the momentum equations and the generation of random stress tensor for a tetrahedron finite element mesh. Numerical results and discussions along with the validations are presented in Sec. IV, and the conclusions are in Sec. V.

II. FORMULATION OF THE PROBLEM

The Brownian motion of a nanoparticle in an incompressible Newtonian fluid contained in a horizontal circular vessel is considered. The fluid and particle equations are formulated in an inertial frame of reference with the origin coinciding with the center of the vessel (Figure 1). The diameter, D, and the length, L, of the vessel (tube) are very large compared to the particle size, d, the diameter of the particle. Two different cases are considered: a fluid at rest in a cylindrical vessel and a fully developed Poiseuille flow in a circular tube. Initially, a nanoparticle is introduced either at the vessel (tube) centerline or at suitably chosen locations away from the center line towards the bounding wall. In the numerical simulation for Poiseuille flow, the particle is initially fixed at the starting location and the flow is allowed to evolve until the flow is

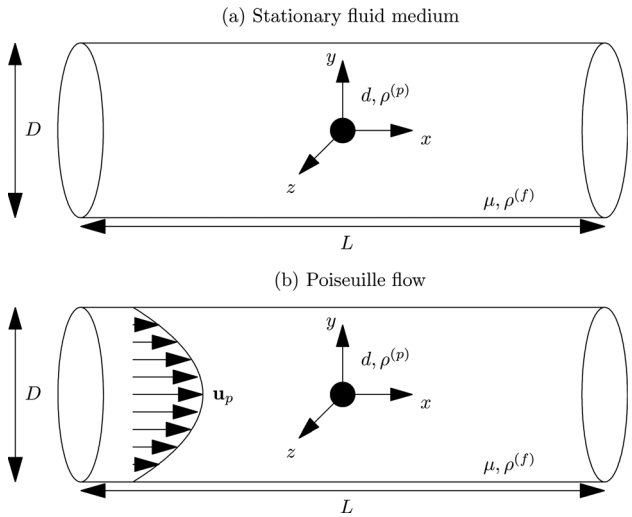

FIG. 1. Schematic representation of a nanoparticle in a cylindrical vessel (tube) (not to scale). Diameter of the tube: $D = 10\,\mu$m; length of the tube: $L = 10\,\mu$m; diameter of the nanoparticle: $d(500\,\text{nm} \le d \le 1000\,\text{nm})$; viscosity of the fluid: $\mu = 10^{-3}\,\text{kg/ms}$; density of the fluid and the nanoparticle: $\rho^{(f)} = 10^3\,\text{kg/m}^3$ and $990\,\text{kg/m}^3 \le \rho^{(p)} \le 1010\,\text{kg/m}^3$. Particle locations away from the center are not displayed in this figure.

fully developed in the entire domain.[28] Then, the particle is released and allowed to move. This way, the velocity profiles in the flow cases are fully developed in the domain of interest, and the calculations are effected in the fully developed regime. No body force is considered either for the particle or for the fluid domain. At time $t = 0$, the nanoparticle is subjected to Brownian motion in each case. The motion of the nanoparticle is determined by the hydrodynamic forces and torques acting on the particle and the wall interactions.

A. Governing equations and boundary conditions

The motion of an incompressible Newtonian fluid satisfies the conservation of mass and momentum given by

$$\nabla \cdot \mathbf{u} = 0, \tag{1}$$

$$\rho^{(f)} \frac{D\mathbf{u}}{Dt} = \nabla \cdot \boldsymbol{\sigma}, \tag{2}$$

where $\mathbf{u}$ and $\rho^{(f)}$ are the velocity and density of the fluid, respectively, and $\boldsymbol{\sigma}$ is the stress tensor. The material derivative of the velocity in Eq. (2) is given by

$$\frac{D\mathbf{u}}{Dt} = \frac{\partial \mathbf{u}}{\partial t} + (\mathbf{u} \cdot \nabla)\mathbf{u}. \tag{3}$$

For a Newtonian fluid, the stress tensor is given by

$$\boldsymbol{\sigma} = -p\mathbf{J} + 2\mu\mathbf{D}[\mathbf{u}] + \mathbf{S}; \quad \mathbf{D}[\mathbf{u}] = \frac{1}{2}[\nabla\mathbf{u} + (\nabla\mathbf{u})^T], \tag{4}$$

where p is the pressure, $\mathbf{J}$ is the identity tensor, μ is the dynamic viscosity, $\mathbf{D}[\mathbf{u}]$ is the rate of deformation tensor, and $\mathbf{S}$ is the random stress tensor. $\mathbf{S}$ is assumed to be a Gaussian with

$$\begin{aligned} \langle S_{ij}(\mathbf{x},t)\rangle &= 0 \quad \& \\ \langle S_{ik}(\mathbf{x},t)S_{lm}(\mathbf{x}',t')\rangle &= 2k_B T\mu(\delta_{il}\delta_{km} + \delta_{im}\delta_{kl})\delta(\mathbf{x}-\mathbf{x}')\delta(t-t'), \end{aligned} \tag{5}$$

where $\langle\ \rangle$ is the ensemble average, k_B is the Boltzmann constant, T is the absolute temperature, δ_{ij} is the Kronecker delta, and the Dirac delta function $\delta(\mathbf{x}-\mathbf{x}')$ denotes that the components of the random stress tensor are spatially uncorrelated (Markovian). The right hand side of Eq. (5) shows that the mean and variance of the thermal fluctuations are chosen to be consistent with the fluctuation-dissipation theorem[4,20,21,45] for an incompressible fluid. By including this stochastic stress tensor due to the thermal fluctuations in the governing equations, the macroscopic hydrodynamic theory is generalized to include the relevant physics of the mesoscopic scales ranging from tens of nanometers to a few microns.

For a rigid particle suspended in an incompressible Newtonian fluid, the translational motion of the particle satisfies Newton's second law,

$$m\frac{d\mathbf{U}}{dt} = \mathbf{F}, \tag{6}$$

and the rotational motion satisfies the Euler equation,

$$\frac{d(\mathbf{I}\boldsymbol{\omega})}{dt} = \mathbf{T}, \tag{7}$$

where m is the mass of the particle, $\mathbf{I}$ is its moment of inertia, and $\mathbf{U}$ and $\boldsymbol{\omega}$ are the translational and angular velocities of the particle, respectively. The hydrodynamic force $\mathbf{F}$ and the torque $\mathbf{T}$ acting on the particle are given by

$$\mathbf{F} = -\int_{\partial\Sigma_p} \boldsymbol{\sigma}\cdot\hat{\mathbf{n}}\, ds; \quad \mathbf{T} = -\int_{\partial\Sigma_p} (\mathbf{x}-\mathbf{X}) \times (\boldsymbol{\sigma}\cdot\hat{\mathbf{n}}) ds, \tag{8}$$

where $\mathbf{X}$ is the position of the centroid of the particle, $(\mathbf{x}-\mathbf{X})$ is a vector from the center of the particle to a point on its surface, $\partial\Sigma_p$ denotes the particle surface, and $\hat{\mathbf{n}}$ is the unit normal vector on the surface of the particle pointing into the particle.

The initial conditions for the problem are

$$\mathbf{U}(t=0) = 0 \quad \mathbf{u}(t=0) = 0 \quad \text{on} \quad \Sigma_0 - \partial\Sigma_i, \tag{9}$$

and the boundary conditions are given by

$$\mathbf{u} = \mathbf{u}_p \quad \text{on} \quad \partial\Sigma_i, \tag{10}$$

$$\boldsymbol{\sigma}\cdot\hat{\mathbf{n}} = 0 \quad \text{on} \quad \partial\Sigma_o, \tag{11}$$

$$\mathbf{u} = \mathbf{U} + \boldsymbol{\omega}\times(\mathbf{x}-\mathbf{X}) \quad \text{on} \quad \partial\Sigma_p, \tag{12}$$

where $\mathbf{u}_p$ is the prescribed velocity (zero or fully developed Poiseuille flow inlet profile), Σ_0 is the domain occupied by the fluid, and $\partial\Sigma_i$ and $\partial\Sigma_o$ are the inlet and outlet boundaries, respectively. The stochastic governing equations (1)–(7) along with the initial and boundary conditions (9)–(12) are solved numerically. It is assumed that there is no body torque acting at any point in the fluid and the viscous stress tensor, $\boldsymbol{\sigma}$, is symmetric. The fluctuation-dissipation theorem for the random stress tensor of the fluid requires that $\mathbf{S}$ is symmetric as well.[21,46]

III. COMBINED FLUID-SOLID WEAK FORMULATION

Owing to the complex nature of the shape of the fluid-particle domain, finite-element techniques are particularly useful for discretizing the governing fluid equations. For this purpose, a weak formulation that incorporates both the fluid and particle equations (1), (2), (6), and (7) is considered.[22,23,27,29]

Let, $\mathbb{V}$ be the function space given by

$$\mathbb{V} = \left\{ \begin{array}{l} \mathbf{V} = (\mathbf{u},\mathbf{U},\boldsymbol{\omega}) | \mathbf{u} \in H^1, (\mathbf{U},\boldsymbol{\omega}) \in \mathcal{R}^3, \\ \mathbf{u} = \mathbf{U} + \boldsymbol{\omega}\times(\mathbf{x}-\mathbf{X}) \text{ on } \partial\Sigma_p \text{ and } \mathbf{u} = \mathbf{u}_p \text{ on } \partial\Sigma_i. \end{array} \right\}. \tag{13}$$

Here, Hilbert space H^1 is defined on the fluid domain, and the particle velocities belong to the three dimensional real space $\mathcal{R}^3$. The square integrable $L2$ -functions in an L^2 space is chosen for the pressure and is denoted by

$$\mathbb{P} = \{p | p \in L^2\}. \tag{14}$$

The test function $\mathbf{V}$ (variation) is considered as follows to derive the weak formulation for the combined fluid-particle system,

$$\tilde{\mathbf{V}} = (\tilde{\mathbf{u}}, \tilde{\mathbf{U}}, \tilde{\boldsymbol{\omega}}) \in \mathbb{V}_0. \tag{15}$$

Here, the variational space $\mathbb{V}_0$ is the same as $\mathbb{V}$, except that $\mathbf{u} = 0$ on $\partial\Sigma_i$. Multiplying Eq. (2) by the test function for the fluid velocity, $\tilde{\mathbf{u}}$, and integrating over the fluid domain at time t gives

$$\int_{\Sigma_0} \rho^{(f)} \frac{D\mathbf{u}}{Dt} \cdot \tilde{\mathbf{u}}\, dV + \int_{\Sigma_0} \boldsymbol{\sigma} : \nabla\tilde{\mathbf{u}} dV - \int_{\partial\Sigma_p} (\boldsymbol{\sigma}\cdot\hat{\mathbf{n}})\cdot\tilde{\mathbf{u}}\, ds = 0. \tag{16}$$

It should be noted that the variations for each variable introduced above are arbitrary except on the particle surface, where the no-slip boundary condition (12) enforces the equality of variations of fluid and particle velocities given by the following relation

$$\tilde{\mathbf{u}} = \tilde{\mathbf{U}} + \tilde{\boldsymbol{\omega}} \times (\mathbf{x} - \mathbf{X}) \text{ on } \partial\Sigma_p. \tag{17}$$

Using the equations of motion for the particles (6) and (7), the surface integral in Eq. (16) may be rewritten as follows:

$$\begin{aligned} -\int_{\partial\Sigma_p} (\boldsymbol{\sigma}\cdot\hat{\mathbf{n}})\cdot\tilde{\mathbf{u}}\, ds &= -\tilde{\mathbf{U}}\cdot\int_{\partial\Sigma_p} (\boldsymbol{\sigma}\cdot\hat{\mathbf{n}}) ds \\ &\quad - \tilde{\boldsymbol{\omega}}\cdot\int_{\partial\Sigma_p} (\mathbf{x}-\mathbf{X})\times(\boldsymbol{\sigma}\cdot\hat{\mathbf{n}}) ds \\ &= \tilde{\mathbf{U}}\cdot\left[m\frac{d\mathbf{U}}{dt}\right] + \tilde{\boldsymbol{\omega}}\cdot\left[\mathbf{I}\frac{d\boldsymbol{\omega}}{dt}\right]. \end{aligned} \tag{18}$$

Substituting for stress tensor $\boldsymbol{\sigma}$ from Eqs. (4) and (18) into Eq. (16), the combined fluid-particle momentum equation for the fluctuating hydrodynamics method is given by

$$\begin{aligned} &\int_{\Sigma_0} \rho^{(f)} \frac{D\mathbf{u}}{Dt}\cdot\tilde{\mathbf{u}} dV - \int_{\Sigma_0} p(\nabla\cdot\tilde{\mathbf{u}}) dV \\ &\quad + \int_{\Sigma_0} \left\{\mu\left[\nabla\mathbf{u} + (\nabla\mathbf{u})^T\right] + \mathbf{S}\right\} : \nabla\tilde{\mathbf{u}}\, dV \\ &\quad + \tilde{\mathbf{U}}\cdot\left[m\frac{d\mathbf{U}}{dt}\right] + \tilde{\boldsymbol{\omega}}\cdot\left[\mathbf{I}\frac{d\boldsymbol{\omega}}{dt}\right] = 0. \end{aligned} \tag{19}$$

The weak formulation for the mass conservation equation is obtained in a similar fashion. Let, $\tilde{p}$ be the variation of pressure p such that $\tilde{p} \in \mathbb{P}$. Here, the function space for both $\tilde{p}$ and p are chosen to be the same. The weak form of Eq. (1) is then given by

$$\int_{\Sigma_0} \tilde{p}(\nabla\cdot\mathbf{u}) dV = 0. \tag{20}$$

The domain movement is handled by an ALE scheme. The details of mesh, its movement techniques, temporal discretization of time derivatives, and spatial discretization of the domain are described below.

A. Random stress tensor for the tetrahedral finite element mesh

Following Hu,[22] Hu *et al.*,[23] and Hughes *et al.*,[47] the computational domain is covered by a finite element mesh generated using Delaunay-Voronoi methods. In this study, the fluid domain is discretized by quadratic irregular tetrahedral elements. Since the stochastic stresses in Eq. (19) are fundamental to this problem, we now describe the procedure for numerical simulation of the random stresses associated with the unstructured tetrahedron mesh while conserving the volume. A typical element is shown in Figure 2. Figure 3 shows a triangular mesh discretizing the surface of the fluid domain (cylinder) and the surface of the nanoparticle. The discretization of the fluid domain changes at each time step of the simulation due to the motion of the nanoparticle.

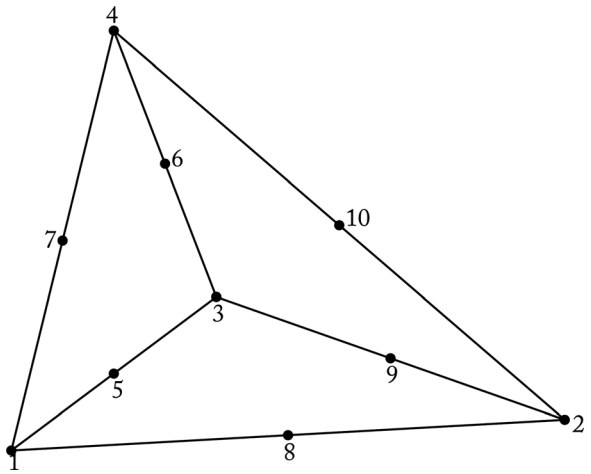

FIG. 2. Representation of a 10-node tetrahedron.

Let V be the total volume of the system. The volume of each quadratic tetrahedral element V_e depends on the state of the mesh. The variance of the random stress tensor (Eq. (5)) depends on this volume element. The random stress tensor is generated per tetrahedral element based on its volume such that total volume of the system

$$V \simeq \sum_{i=1}^{N_e} V_e^{(i)} \tag{21}$$

is conserved, where $V_e^{(i)}$ represents the volume of the ith tetrahedral element and N_e is the number of elements in the finite element mesh. Each quadratic tetrahedron element has four vertices (numbered $1-4$ in Figure 2) and six middle nodes (numbered $5-10$ in Figure 2).

The random stress tensor $\mathbf{S}$ from Eq. (5) in each tetrahedral element becomes

$$\begin{aligned} \langle S_{xx}\rangle &= \langle S_{yy}\rangle = \langle S_{zz}\rangle = 0, \\ \langle S_{xy}\rangle &= \langle S_{yz}\rangle = \langle S_{zx}\rangle = 0, \\ \langle S_{xx}^2\rangle &= \langle S_{yy}^2\rangle = \langle S_{zz}^2\rangle = \frac{4k_BT\mu}{V_e\Delta t}, \\ \langle S_{xy}^2\rangle &= \langle S_{yz}^2\rangle = \langle S_{zx}^2\rangle = \frac{2k_BT\mu}{V_e\Delta t}, \end{aligned} \tag{22}$$

where Δt is the time step for the numerical simulation. Recall that the random stress tensor $\mathbf{S}$ is present in Eq. (19). As

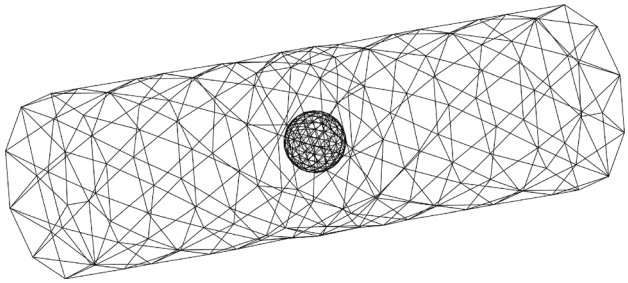

FIG. 3. Finite element surface mesh of a cylindrical tube with one spherical nanoparticle.

stated earlier, an unstructured finite element mesh enables a significantly higher number of mesh points near the nanoparticle and wall surfaces compared to regions far away. As a result, the volume of the tetrahedral elements closer to the particle is much smaller than the elements far away.

B. Mesh movement: ALE technique

When a nanoparticle moves in a fluid medium, the domain of interest occupied by the fluid is irregular and changes with time. An ALE technique has been used to handle the movement of this domain. The material derivative of $\mathbf{u}(\mathbf{x},t)$ in an ALE formulation is given as

$$\frac{D\mathbf{u}}{Dt}(\mathbf{x},t)=\frac{\delta\mathbf{u}}{\delta t}+[(\mathbf{u}-\mathbf{u}_m)\cdot\nabla]\mathbf{u}, \tag{23}$$

where

$$\frac{\delta\mathbf{u}}{\delta t}=\frac{\partial}{\partial t}\mathbf{u}(\mathbf{x}(\varphi,t),t)\bigg|_{\varphi\ is\ fixed} \quad \text{and} \quad \frac{d}{dt}\mathbf{x}(\varphi,t)=\mathbf{u}_m \tag{24}$$

are, respectively, the referential time derivative and the mesh velocity (domain velocity). The function $\mathbf{x}(\varphi,t)$ is the mapping from the fixed referential frame to the spatial domain $\Sigma_0(t)$, domain occupied by the fluid at a given time instant t. When the referential and spatial domains coincide at the current instant, $\mathbf{u}_m=0$, the referential time derivative in Eq. (23) reduces to the local Eulerian time derivative. When the mesh velocity coincides with the particle velocity, $\mathbf{u}_m=\mathbf{u}$, the referential time derivative in Eq. (23) regains the Lagrangian time derivative.

The mesh velocity in Eq. (24) is arbitrary in the interior of the domain. The mesh velocity on the boundaries has to follow the motion of the particle and the motion of the confining fluid geometry. The movement of all the interior vertices is computed using the Laplace's equation

$$\nabla\cdot(\varepsilon_e\nabla\mathbf{u}_m)=0 \quad \text{in} \quad \Sigma(t), \tag{25}$$

$$\mathbf{u}_m=\mathbf{U}+\boldsymbol{\omega}\times(\mathbf{x}-\mathbf{X}) \quad \text{on} \quad \partial\Sigma_p, \tag{26}$$

$$\mathbf{u}_m=(\mathbf{U}\cdot\hat{i})\hat{i} \quad \text{on} \quad \partial\Sigma_i\ \&\ \partial\Sigma_o, \tag{27}$$

$$\mathbf{u}_m=(\mathbf{U}\cdot\hat{i})\hat{i} \quad \text{on} \quad \partial\Sigma_w, \tag{28}$$

where $\partial\Sigma_w$ denotes the tube wall and $\hat{i}$ is a unit vector along the axis of the tube. The volume of the tetrahedral elements closer to the particle is much smaller than the elements far away. Here, function ε_e controls the deformation of the mesh, such that the regions away from the particle absorb most of the deformation, while the region close to the particle is relatively stiff. We choose $\varepsilon_e=1/V_e$, where V_e is the volume of the quadratic tetrahedral element. Similarly, the acceleration field, $\mathbf{a}_m(\mathbf{x},t)$, of the mesh vertices is chosen to satisfy

$$\nabla\cdot(\varepsilon_e\nabla\mathbf{a}_m)=0 \quad \text{in} \quad \Sigma(t), \tag{29}$$

$$\mathbf{a}_m=\frac{d\mathbf{U}}{dt}+\frac{d\boldsymbol{\omega}}{dt}\times(\mathbf{x}-\mathbf{X})-\boldsymbol{\omega}\times\mathbf{U} \quad \text{on} \quad \partial\Sigma_p, \tag{30}$$

$$\mathbf{a}_m=\left(\frac{d\mathbf{U}}{dt}\cdot\hat{i}\right)\hat{i} \quad \text{on} \quad \partial\Sigma_i\ \&\ \partial\Sigma_o, \tag{31}$$

$$\mathbf{a}_m=\left(\frac{d\mathbf{U}}{dt}\cdot\hat{i}\right)\hat{i} \quad \text{on} \quad \partial\Sigma_w. \tag{32}$$

This mesh acceleration field is used for the second order mesh movement scheme. The position of the particle and the nodal points of the mesh are updated explicitly. Particle and fluid velocities are calculated semi-implicitly. This explicit-implicit scheme is numerically unconditionally stable. The weak formulations for Eqs. (25) and (29) are obtained in a way similar to that outlined in Sec. III.

C. Spatial and temporal discretization

A numerical simulation at a mesoscopic scale involving a particle in a fluid could be based on a discretization of the Eqs. (1)–(7). However, the discrete forms have to satisfy the fluctuation-dissipation theorem.[6,18–21,48,49] Español and Zúñiga[50] and Español *et al.*[30] have shown that a well behaved set of discrete equations obtained in terms of the finite element shape functions based on the Delaunay triangulation conserves mass, momentum, and energy while ensuring thermodynamic consistency. Furthermore, Español *et al.*[30] have cast their discrete hydrodynamic equations in the GENERIC structure and observed that the resulting reversible matrix does not satisfy the Jacobi identity and the degeneracy conditions of GENERIC structure.[20,21] But, these conditions are of the order of the cell size and vanish in the continuum limit.[30] In effect, Español *et al.*[30] have shown that the finite element discretization procedure based on Delaunay triangulation is an appropriate procedure for discretizing the compressible fluctuating Navier-Stokes equations. In the present study, we obtain the discrete hydrodynamic equations using finite element shape functions based on the Delaunay-Voronoi tetrahedrizations.

The fluid domain is discretized by quadratic tetrahedral finite-elements (10 nodes defined per tetrahedron with 10 basis functions that are second-order polynomials; see Figure 2). The discrete solution for the fluid velocity is approximated in terms of piecewise quadratic functions and is assumed to be continuous over the domain (P2 elements). The discrete solution for the pressure is taken to be piecewise linear and continuous (P1 element). This P1/P2 element for the pressure and the velocity is consistent with the Ladyzhenskaya-Babuska-Brezzi (LBB) or inf-sup condition and yields convergent solutions.[22,23] The pressure and the velocities of the fluid are associated with each node in the system, and the thermal noise (random stresses) is associated with each subelement in the system. The white noise property of stochastic stress tensor is implemented as an absence of correlations between different subelements.[30]

The time derivatives in the combined fluid-solid weak formulation are discretized using a finite difference second-order Crank-Nicolson scheme. The time derivatives in Eq. (19) are replaced by the following expressions:

$$\frac{D\mathbf{u}}{Dt}(\mathbf{x},t_{n+1})\approx 2\frac{\mathbf{u}(\mathbf{x},t_{n+1})-\mathbf{u}(\mathbf{x}',t_n)}{\Delta t}-\frac{\delta\mathbf{u}}{\delta t}(\mathbf{x}',t_n)+[(\mathbf{u}(\mathbf{x},t_{n+1})-\mathbf{u}_m(\mathbf{x},t_{n+1}))\cdot\nabla]\mathbf{u}(\mathbf{x},t_{n+1}), \tag{33}$$

$$\frac{d\mathbf{U}}{dt}(t_{n+1})\approx 2\frac{\mathbf{U}(t_{n+1})-\mathbf{U}(t_n)}{\Delta t}-\frac{d}{dt}\mathbf{U}(t_n), \tag{34}$$

$$\frac{d}{dt}(\mathbf{I}\boldsymbol{\omega})(t_{n+1}) \approx 2\frac{(\mathbf{I}\boldsymbol{\omega})(t_{n+1}) - (\mathbf{I}\boldsymbol{\omega})(t_n)}{\Delta t} - \frac{d}{dt}(\mathbf{I}\boldsymbol{\omega})(t_n), \quad (35)$$

where $\Delta t = t_{n+1} - t_n$ and $\mathbf{x} = \mathbf{x}' + \mathbf{u}_m(\mathbf{x}', t_n)\Delta t + \mathbf{a}_m(\mathbf{x}', t_n)\frac{(\Delta t)^2}{2}$. In order to prevent the distortion of the shape of the rigid particle during simulation, the nodes on the particle surface are reset to the surface at each time step.

The translational and rotational motions of the particle are updated using a second order explicit method as

$$\mathbf{X}(t_{n+1}) = \mathbf{X}(t_n) + \Delta t\mathbf{U}(t_n) + \frac{(\Delta t)^2}{2}\frac{d\mathbf{U}}{dt}(t_n), \quad (36)$$

$$\boldsymbol{\theta}(t_{n+1}) = \boldsymbol{\theta}(t_n) + \Delta t\boldsymbol{\omega}(t_n) + \frac{(\Delta t)^2}{2}\frac{d\boldsymbol{\omega}}{dt}(t_n). \quad (37)$$

For a given finite element mesh and with the finite element interpolation functions as described above, the combined fluid-solid weak formulations (19) and (20) would reduce to a nonlinear system of algebraic equations, which is solved by a Newton-Raphson algorithm. Similarly, the weak formulations for the mesh velocity (25) and the mesh acceleration (29) are also reduced to linear systems of algebraic equations. These linear system of algebraic equations are solved using a biconjugate gradient stabilized algorithm.[51]

D. Time scales

The time scale for the computation of the Brownian motion of the particle may be derived from evaluating the various time scales (macroscopic and mesoscopic) governing the problem. The different time scales involved in this study are (i) hydrodynamic time scale, $\tau_\nu = a^2/\nu$ (the time scale for momentum to diffuse over a distance equal to the radius of the nanoparticle); Brownian time scales, (ii) $\tau_b = m/\zeta^{(t)}$ (Brownian relaxation time over which velocity correlations decay in the Langevin equation), and (iii) $\tau_d = a^2\zeta^{(t)}/k_BT$ (Brownian diffusion time over which the nanoparticle diffuses over a distance equal to its radius). Here, a is the radius of the nanoparticle, ν is the kinematic viscosity, and $\zeta^{(t)} = 6\pi\mu a$ is the Stokes dissipative friction force coefficient for a sphere.

It is noted that the time scales encountered in this problem are such that $\tau_b < \tau_\nu < \tau_d$. For a nanoparticle of radius 250 nm, $\tau_b \approx 1.38 \times 10^{-8}$ s, $\tau_\nu \approx 6.25 \times 10^{-8}$ s, and $\tau_d \approx 6.88 \times 10^{-2}$ s. As a consequence, the relevant time scales for the Brownian motion of a nanoparticle in an incompressible fluid can span many orders of magnitude. In this study, the time step for the numerical simulation Δt has been chosen such that the combined fluid-particle system reproduces the expected Brownian behavior (equipartition theorem, algebraic decay of VACF) arising due to thermal fluctuations. It is required that Δt be smaller than the smallest of all the physical time scales. The simulations presented in this study have been carried out for long enough durations to allow for the temperature of the particle to equilibrate—*i.e.*, if N is the number of simulated time steps then $N \cdot \Delta t = t \gg \tau_\nu$.

IV. NUMERICAL RESULTS AND DISCUSSION

In this section, we numerically predict (i) the translational and rotational temperatures of the nanoparticle with and without bulk flow; the temperature calculation is carried out till thermal equilibration is obtained between the particle and the fluid medium; (ii) the translational and rotational temperatures of nearly neutrally buoyant Brownian particles, thermally equilibrated, in a quiescent fluid; (iii) the translational and rotational velocity distributions of the nanoparticle motion with and without bulk flow; (iv) the translational and rotational VACFs in a quiescent fluid; (v) the translational and rotational mean square displacements (MSD) of the particle in a quiescent fluid, both for ballistic and diffusive regimes; (vi) the effects of the presence of the bounding wall on particles of different radii initially placed at various locations are evaluated for several cases with and without bulk flow; and (vii) provide the computational cost for fluctuating hydrodynamics. The various numerical predictions have been compared with analytical and experimental results, where available.

A solid spherical particle of radius $a = 250$ nm is initially placed at the center of a cylindrical tube ($R = 5\,\mu$m) containing a Newtonian fluid. Both, quiescent and fully developed Poiseuille flows are considered. The computational domain moves with the particle, and from the particle location, the ends of the computational domain are at a distance of $20a$ at any instant of time.[27] For a Poiseuille flow, the prescribed velocity $\mathbf{u}_p = U_{max}(1 - r^2/R^2)\hat{i}$, where U_{max} is the maximum fluid velocity, and r is the radial distance of the tube from the center line (x-axis). As mentioned earlier, the particle is initially fixed at the starting location and the flow is allowed to evolve until the flow is fully developed in the entire domain.[28] The time taken for the flow to fully develop over the entire computational domain is $t/\tau_\nu = 24$. Now, the time is reset to zero and the particle is released. Figure 4 shows the fully developed analytical and the numerical profiles for Poiseuille flow in the cylindrical tube. The physical parameters used are $k_B = 1.3806503 \times 10^{-23}$ kg m^2/s^{2}K; $\mu = 10^{-3}$ kg/ms; $\rho^{(f)} = 10^3$ kg/m^3; and five particle densities in the range, 990 kg/m^3 $\leq \rho^{(p)} \leq$ 1010 kg/m^3. The temperature of the fluid is initially set to $T = 310$ K and the particle at zero Kelvin. The maximum fluid velocities (for Poiseuille flow) presented in this study range from $U_{max} = 10^{-4}$ to 10 mm/s, relevant to some biological applications.[37] The flow Reynolds number ($Re_f = \rho^{(f)}RU_{max}/\mu$) ranges from 5×10^{-7} to 5×10^{-2} for Poiseuille flow. The particle Reynolds number ($Re_p = \rho^{(f)}aU_{max}/\mu$) ranges from 2.5×10^{-8} to 2.5×10^{-3} for Poiseuille flow. Before the introduction of the nanoparticle, we have ascertained that the solutions to the continuum equations of fluctuating hydrodynamics (Eqs. (1)–(5)) reproduce the Gaussian field with regard to the distribution of fluid velocities in confirmation with results of Donev *et al.*[7]

For a given nanoparticle of radius a and tube radius R, a "realization" consists of N time steps (approximately 10 s wall clock time for each time step that is generally considered in this study). The number of time steps depends upon equilibration of particle temperature or determination of VACFs and MSD. In order to ensure the uniqueness of the realizations, different initial seeds are chosen for a Gaussian random number generator.

A. Temperature of the nanoparticle

From the equipartition theorem, at thermal equilibrium, the translational and rotational temperatures of the nanoparticle are given by

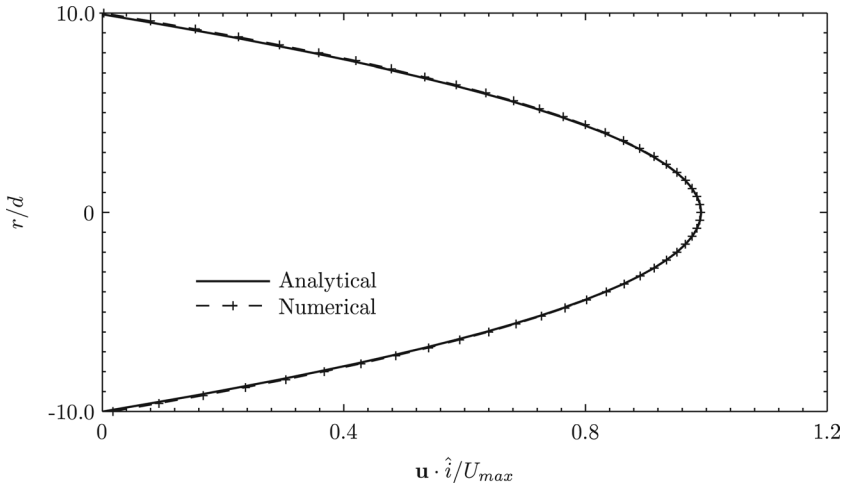

FIG. 4. Analytical and computational profiles for Poiseuille flow in the *xy* slice. Profiles at inlet, outlet, and in the flow domain, in the absence of the particle are the same as shown here.

$$T^{(t)} = \frac{m\langle \mathbf{U}^2 \rangle}{3k_B}; \quad T^{(r)} = \frac{\mathbf{I}\langle \boldsymbol{\omega}^2 \rangle}{3k_B}. \tag{38}$$

Since we have considered an incompressible fluid, in our simulations, to account for compressibility effects, the particle mass m is augmented by an added mass $m_0/2$, where m_0 is the mass of the displaced fluid. In other words, the particle will respond to an imposed force as if its mass were $M = m + m_0/2$, where M is the virtual or added mass of the particle.[33,34,36] The rotational motion of the nanoparticle is unaffected by the incompressibility of the fluid. With the incompressibility assumption, the translational and rotational temperatures of the fluctuating nanoparticle are evaluated from

$$T^{(t)} = \frac{M\langle \mathbf{U}^2 \rangle}{3k_B}; \quad T^{(r)} = \frac{\mathbf{I}\langle \boldsymbol{\omega}^2 \rangle}{3k_B}. \tag{39}$$

Figure 5 shows the time evolution of the ensemble average of the mean square translational and rotational velocities of neutrally buoyant particle ($a = 250\,\text{nm}$), normalized by $3k_BT/M$ and $3k_BT/\mathbf{I}$, respectively, in a stationary fluid medium. These are obtained from five different realizations in each coordinate direction. Each realization consists of $N = 20\,000$ time steps. Thus, to evaluate the equilibration of the particle temperature with the preset fluid temperature, we have employed $3 \times 5 \times 20\,000 = 300\,000$ time steps. The temperatures characterizing translational and rotational motion of the particle agree with the preset temperature of the fluid within 5% error, after an initial transient. Furthermore, the number of realizations case has been arrived such that any further increase in the number of realizations does not significantly change the prediction of temperature equilibration.

Figure 6 shows the translational and rotational temperatures of the particle in a stationary medium as a function of the normalized surface mesh length (mesh length divided by particle radius) for two different values of the step size Δt. The error bars have been plotted from standard deviations of the temperatures obtained with 15 different realizations (5

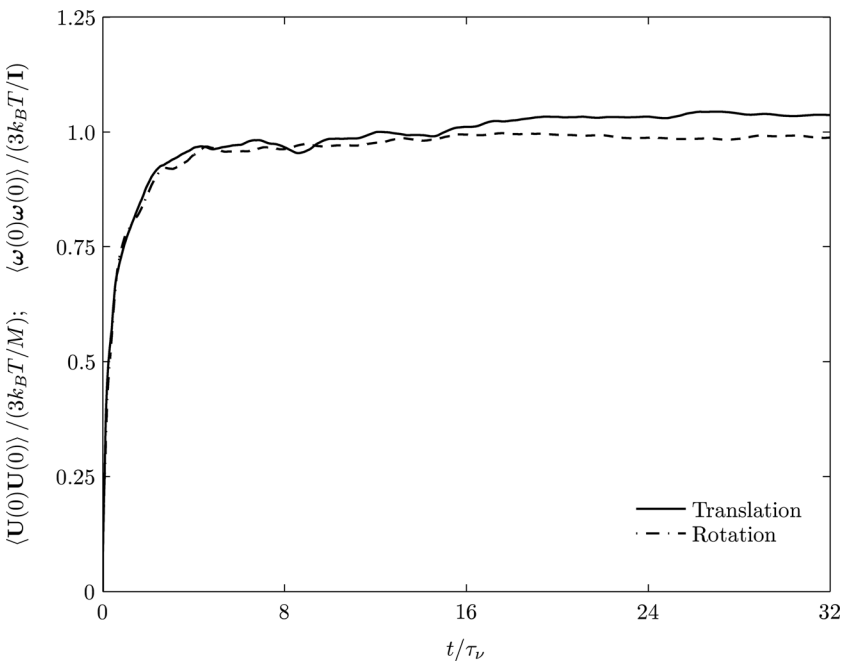

FIG. 5. Time evolution of the mean square translational and rotational velocities of neutrally buoyant particle ($a = 250$ nm) normalized by $3k_BT/M$ and $3k_BT/\mathbf{I}$, respectively, in a stationary fluid medium.

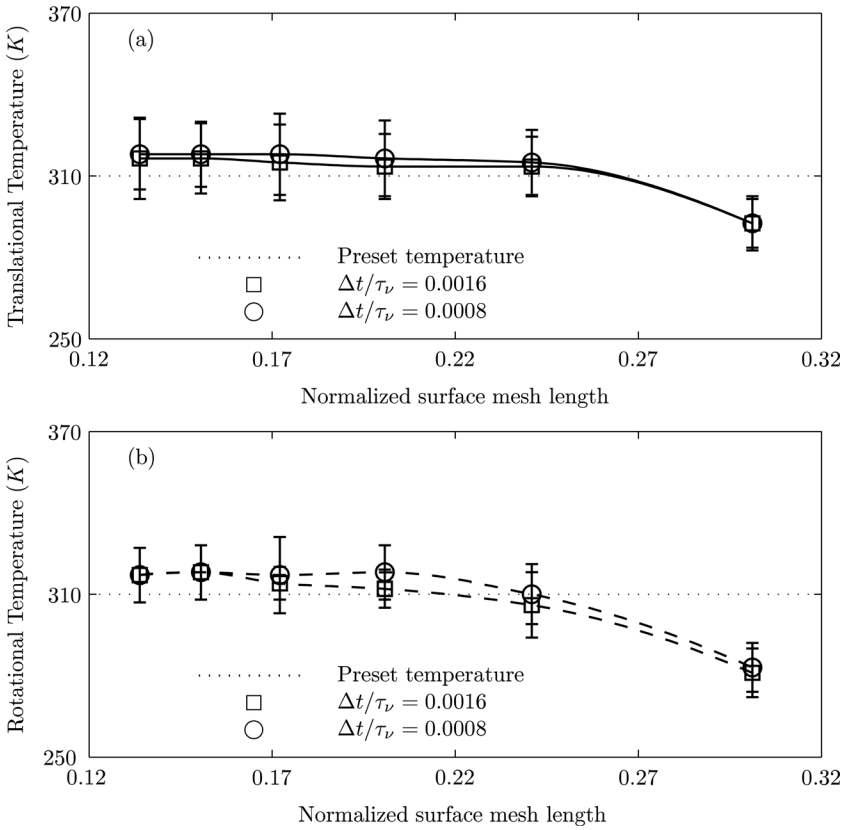

FIG. 6. Translational and rotational temperatures of the nanoparticle as a function of the normalized surface mesh length (mesh length divided by particle radius) for two different values of the computational time Δt in a stationary Newtonian fluid medium. The preset temperature is 310 K, and $\Delta t/\tau_\nu = 0.0016, 0.0008$, $\rho^{(p)}/\rho^{(f)} = 1$.

realizations in each direction). For a given Δt, convergence is noted as the normalized mesh size is decreased. Furthermore, for the appropriately chosen values of Δt, the convergence in the temperature is also noted. It is observed that translational and rotational temperatures of the nanoparticle agree with the preset temperature to within 5% error.

Figure 7 shows that translational and rotational temperatures of nearly neutrally buoyant Brownian particles, thermally equilibrated, in a quiescent fluid medium are independent of the density of the particle in relation to that of fluid. This has been discussed in Hauge and Martin-Löf,[45] although no quantitative results specific to this issue are provided there.

Figure 8 shows the translational and rotational temperature equilibration of a nanoparticle initially placed at the center of a cylindrical tube as a function of the particle Reynolds number for Poiseuille flow. A convergence in the observed temperature is achieved for $\Delta t = 0.0016$. It is observed that the calculated temperature of the nanoparticle in the Poiseuille flow is essentially independent of the fluid velocity for the range of Reynolds numbers investigated and agrees with the preset temperature ($< 5\%$ error).

B. Velocity of the nanoparticle

At thermal equilibrium, the probability distribution of the velocity of the fluctuating nanoparticle follows the Boltzmann distribution. The equilibrium statistics of the three components of $\mathbf{U}$ and $\boldsymbol{\omega}$ along the three coordinate directions are independent of each other.

The apparent translational and rotational velocities of the nanoparticle are determined as $(\mathbf{U} - \overline{\mathbf{U}})$ and $(\boldsymbol{\omega} - \overline{\boldsymbol{\omega}})$, where $\overline{\mathbf{U}}$ and $\overline{\boldsymbol{\omega}}$ are the average translational and rotational velocities of the particle in the flowing incompressible fluid.

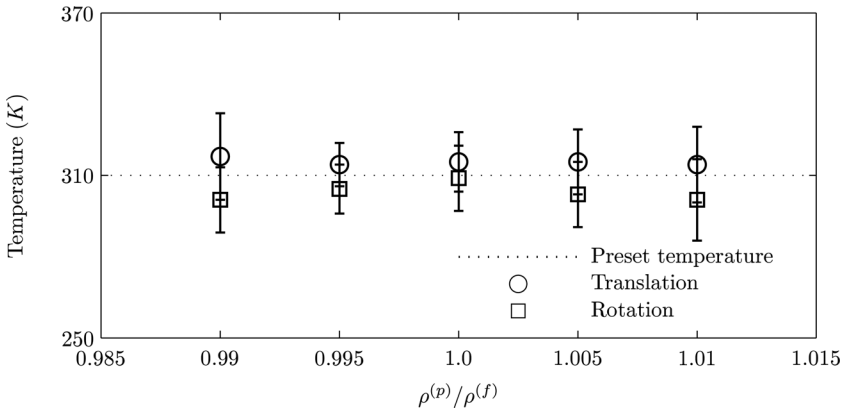

FIG. 7. Translational and rotational temperatures of a nearly neutrally buoyant nanoparticle ($a = 250$ nm) in a stationary fluid medium using fluctuating hydrodynamics approach as a function of the particle density normalized with fluid density.

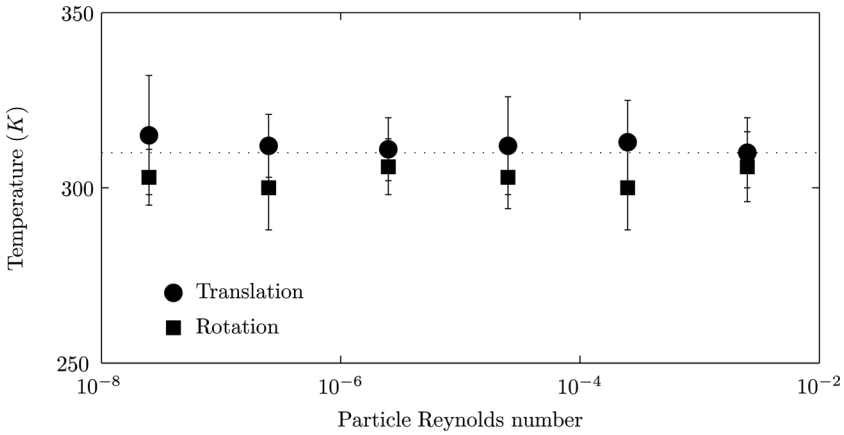

FIG. 8. Translational and rotational temperatures of the nanoparticle ($a = 250\,\text{nm}$) initially placed at the center of a cylindrical tube as a function of particle Reynolds number in Poiseuille flow. The preset temperature is 310 K and $\rho^{(p)}/\rho^{(f)} = 1$.

For determining the velocity distribution of the nanoparticle, 5 realizations in each coordinate direction consisting of $5 \times 20\,000 = 100\,000$ time steps have been computed. Thus, a total of 300 000 time steps have been computed. For the Poiseuille flow in the flow direction, 100 000 time steps have been computed (5 realizations). In Figure 9, the numerically simulated components of $(\mathbf{U} - \overline{\mathbf{U}})$ (Figure 9(a)) and $(\boldsymbol{\omega} - \overline{\boldsymbol{\omega}})$ (Figure 9(b)) (represented by three different symbols) of the nanoparticle with radius $a = 250\,\text{nm}$ are compared with the analytical Maxwell-Boltzmann distribution with a zero mean and variance of k_BT/M and $k_BT/\mathbf{I}$, respectively. It is observed that each degree of freedom individually follows a Gaussian distribution. In particular, the mean and the variance calculated by using the fluctuating hydrodynamics approach agrees within 5% error (see dotted line in Figure 9) with that of the analytical Maxwell-Boltzmann distribution. This validates the numerical procedure employed in this study.

We have also computed that (i) the average velocity of the particle initially placed at the center of the tube in a Poiseuille flow with velocity $U_{max} = 0.01\,\text{m/s}$ $(\mathbf{u}_p|_{r=0} = (0.01, 0.0, 0.0)\,\text{m/s})$ is equal to $\overline{\mathbf{U}}/\sqrt{k_BT/M} = (1.49 \pm 0.05, 0.05 \pm 0.05, 0.004 \pm 0.03)$ and $\overline{\boldsymbol{\omega}}/\sqrt{k_BT/\mathbf{I}} = (0.001 \pm 0.01, 0.006 \pm 0.004, 0.004 \pm 0.004)$, where the $\pm$ quantity denotes standard deviation calculated from five different realizations. The average translational velocity, $\overline{\mathbf{U}}/\sqrt{k_BT/M}$, obtained here is consistent with $\mathbf{u}_p/\sqrt{k_BT/M} = (1.51, 0.0, 0.0)$; (ii) the average velocity of the particle initially placed at $r = 2R/5$ in a Poiseuille flow with velocity $U_{max} = 0.01m/s$ $(\mathbf{u}_p|_{r=2R/5} = (0.0084, 0.0, 0.0)m/s)$ is equal to $\overline{\mathbf{U}}/\sqrt{k_BT/M} = (1.27 \pm 0.02, 0.03 \pm 0.04, 0.04 \pm 0.02)$ and $\overline{\boldsymbol{\omega}}/\sqrt{k_BT/\mathbf{I}} = (0.001 \pm 0.01, 0.005 \pm 0.03, 0.005 \pm 0.146)$. When the particle is placed at $r = 2R/5$ in a Poiseuille flow, the average translational velocity, $\overline{\mathbf{U}}/\sqrt{k_BT/M}$, obtained here is consistent with $\mathbf{u}_p|_{r=2R/5}/\sqrt{k_BT/M} = (1.27, 0.0, 0.0)$ and the average rotational velocity of the particle is consistent with the average angular velocity, $\Omega(= 1/2(d\mathbf{U}/dr)|_{r=2R/5})$, of the particle in Stokes flow, $\Omega/\sqrt{k_BT/\mathbf{I}} = (0.0, 0.0, 0.03)$.

C. VACF of the nanoparticle

A nanoparticle experiencing Brownian motion in a fluid is influenced by the hydrodynamic interactions. The fluid around the particle is dragged in the direction of motion of the particle. On the other hand, the motion of the particle is resisted by viscous forces arising due to its motion relative to the surrounding fluid. The momentum of the fluid surrounding the particle at any instant is related to its recent history. The friction coefficient is time dependent and is no longer given by the constant Stokes value.

Figure 10 shows the VACF of the translational and rotational motions of a nanoparticle ($a = 250\,\text{nm}$) in a quiescent fluid medium in a circular vessel as obtained from our numerical simulations. For determining the VACF of the nanoparticle, 45 ($15 \times 3 = 45$) realizations have been employed with total computation of $45 \times 100\,000 = 4\,500\,000$ time steps. It may be observed that the translational and rotational VACFs of the Brownian particle have power-law decays over long times that are $\sim t^{-3/2}$ and $\sim t^{-5/2}$, respectively.

In this context, Zwanzig and Bixon[33] have shown that for constant friction coefficient $\zeta^{(t)}$, the VACF of the particle in a simple fluid obeys

$$\langle \mathbf{U}(t)\mathbf{U}(0)\rangle = \frac{3k_BT}{M} e^{-\zeta^{(t)}t/M}; \quad \langle \boldsymbol{\omega}(t)\boldsymbol{\omega}(0)\rangle = \frac{3k_BT}{\mathbf{I}} e^{-\zeta^{(r)}t/\mathbf{I}}, \tag{40}$$

which denote exponential decays, while for the time dependent friction coefficient, the decay of the VACF at long times obeys a power-law:[45]

$$\langle \mathbf{U}(t)\mathbf{U}(0)\rangle \simeq \left(\frac{k_BT\rho^{(f)1/2}}{4\pi^{3/2}\mu^{3/2}}\right) t^{-3/2};$$
$$\langle \boldsymbol{\omega}(t)\boldsymbol{\omega}(0)\rangle \simeq \left(\frac{3k_BT\rho^{(f)3/2}}{32\pi^{3/2}\mu^{5/2}}\right) t^{-5/2}. \tag{41}$$

Based on our numerical simulation, for the parameters considered, the translational VACF follows an exponential decay in the range for $t \leq 0.343\tau_\nu$ and an algebraic tail for $t \geq 1.202\tau_\nu$. Our simulation also predicts the transitional range. Similarly, the rotational VACF follows an exponential decay, for $t \leq 0.115\tau_\nu$ and an algebraic tail for $t \geq 0.495\tau_\nu$. Our computed results are in good agreement with the predictions of the above Eqs. (40) and (41) for short and long times, respectively, and also predict the transition between the two. The error bars have been plotted from standard deviations of the decay at particular time instants obtained with 45 different realizations.

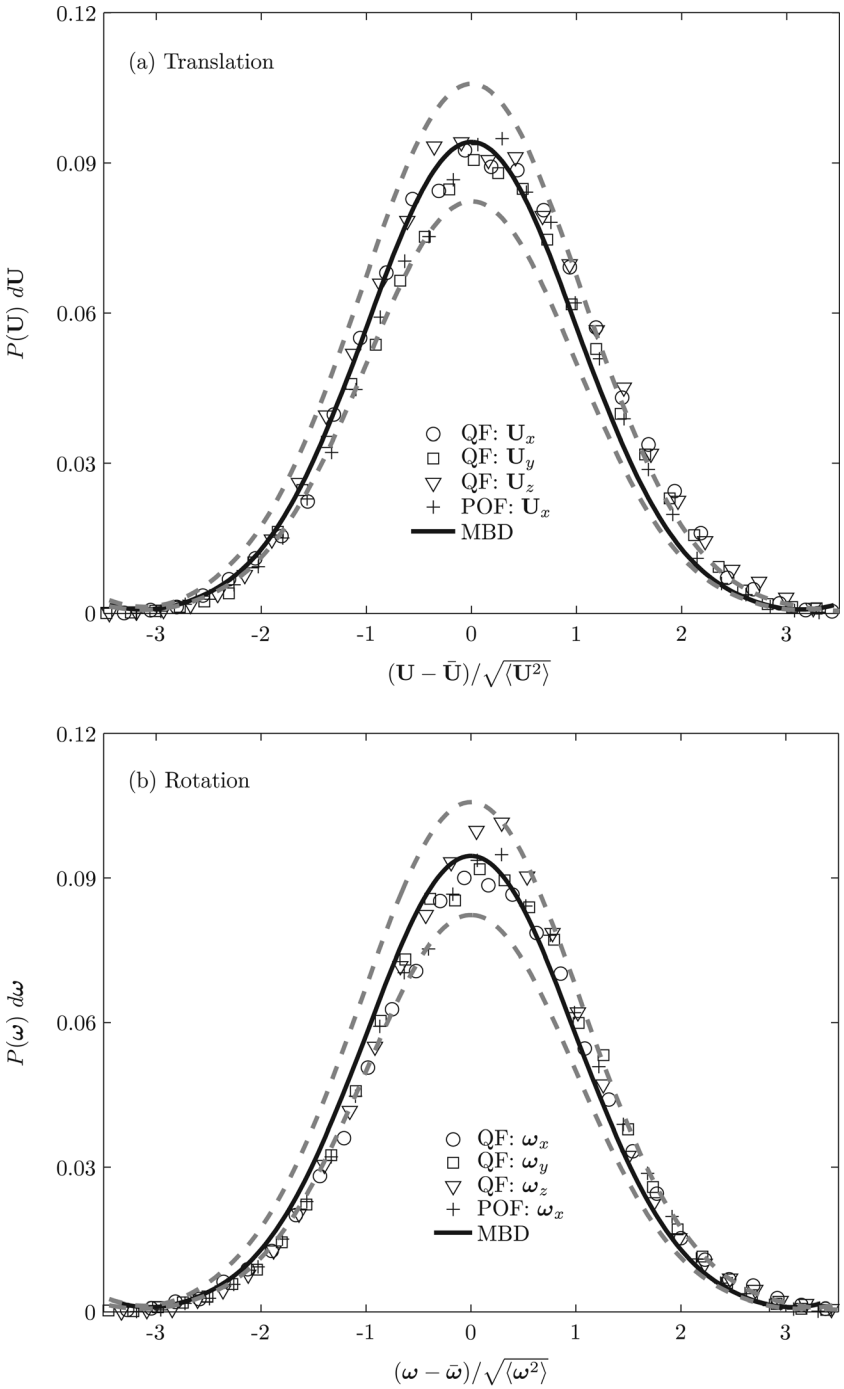

FIG. 9. Equilibrium probability of the (a) translational and (b) rotational velocities of the nanoparticle ($a = 250$ nm) in a Newtonian fluid using fluctuating hydrodynamics for $\rho^{(p)}/\rho^{(f)} = 1$. QF: Quiescent fluid; POF: Poiseuille flow; MBD: Maxwell-Boltzmann distribution.

D. Diffusion of the nanoparticle

Figure 11 shows the numerically obtained translational and rotational MSDs (measures of diffusion) of a neutrally buoyant nanoparticle ($a = 250$ nm) in a quiescent fluid medium, initially placed at the center of the vessel ($R = 5\ \mu$m), for both short and long times. It is observed that in the regime where the particle's motion is dominated by its own inertia (ballistic), $0.346\tau_\nu \le t \le 0.63\tau_\nu$ (translation), and $0.174\tau_\nu \le t \le 0.316\tau_\nu$ (rotation), the translational and rotational motions of the particle follow $(3k_BT/M)t^2$ and $(3k_BT/\mathbf{I})t^2$, respectively. In the diffusive regime, $t \gg \tau_b$, and when $t \ge 7\tau_\nu$ (translation) and $t \ge 1.2\tau_\nu$ (rotation), the translational and rotational MSDs increase linearly in time to follow $6D_\infty^{(t)}t$ and $6D_\infty^{(r)}t$, respectively, where $D_\infty^{(t)} = k_BT/\zeta^{(t)}$ and $D_\infty^{(r)} = k_BT/\zeta^{(r)}$ ($\zeta^{(r)} = 8\pi\mu a^3$) are the translational and rotational self-diffusion coefficients. The MSDs in an intermediate regime between the ballistic and the diffusive are related to hydrodynamic memory effects, and these are also displayed by our simulation. The above numerical estimates were developed from 45 realizations ($3 \times 5 = 45$), each realization computed up to 100 000 time steps.

It is also observed from Figure 11 that in the diffusive regime, the translational and rotational MSDs of the particle follow Stokes-Einstein[52,53] and Stokes-Einstein-Debye[54] relations, respectively. Recently, Huang *et al.*[36] have experimentally investigated the Brownian motion of a single particle in a liquid and provided results for the translational

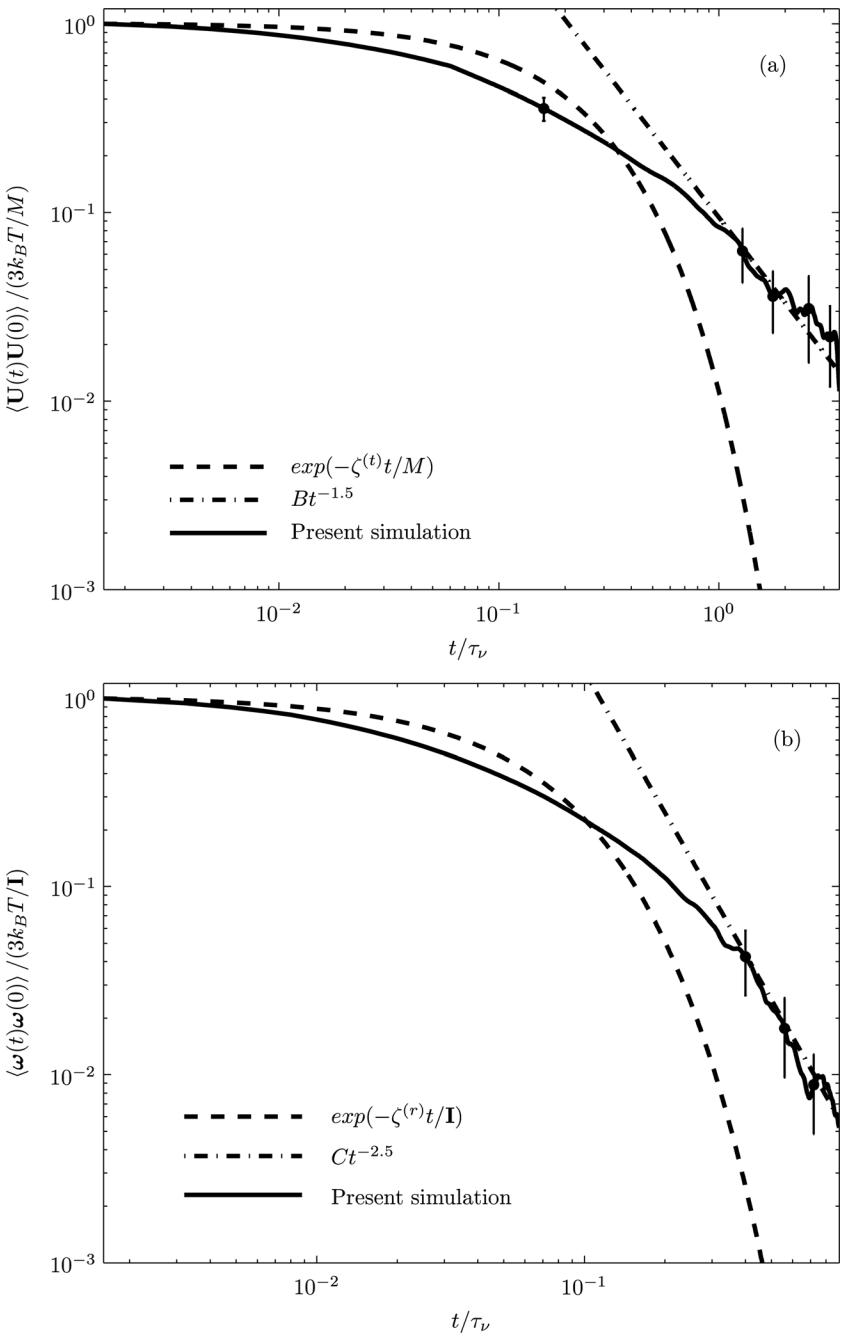

FIG. 10. (a) Translational ($B = M\rho^{(f)1/2}/12\pi^{3/2}\mu^{3/2}$) and (b) rotational ($C = \mathbf{I}\rho^{(f)3/2}/32\pi^{3/2}\mu^{5/2}$) VACFs of a neutrally buoyant Brownian particle ($a = 250\,\text{nm}$) in a stationary fluid medium in a circular vessel ($R = 5\,\mu\text{m}$) using fluctuating hydrodynamics.

MSDs in both the ballistic and the diffusive regimes corresponding to thermal equilibration. Our numerical predictions of ballistic and diffusive motion of a particle in a fluid are in good agreement with Huang *et al.*[36]

E. Wall effects

As stated earlier, our main motivation for the present study is to simulate a nanoparticle thermal motion in a fluid flow that occurs in TDD and similar microparticle flows. In such flows, the hydrodynamic wall effects on the particle diffusivity are relevant. For a particle initially located at the center of the cylindrical vessel, the wall effects play a minimal role ($\leq 3\%$, compared to an unbounded fluid domain) on the diffusion coefficient (see Figure 11).[55] When a particle of radius a is initially placed at a distance h from the tube wall to the center of the particle, $h < R$, the particle-wall interactions modify the particle diffusivity. For $a \ll R$, in a quiescent fluid, the Brownian motion near the vessel wall is similar to that of motion in the vicinity of a plane wall (curvature effects may be neglected).[55,56] For a particle initially located in the near vicinity of the wall, there is reduced space for the surrounding fluid to negotiate the particle and the corresponding drag force in a direction parallel to the wall is higher. The diffusivity of the particle in the proximity of the wall may be estimated to be $D_w^{(t)} = D_\infty^{(t)}(\zeta_w^{(t)}/\zeta^{(t)})^{-1}$ in x, y, and z directions,[57] while $\zeta_w^{(t)}$ depends on the particular direction.

Figure 12 shows the numerically obtained parallel (x direction) and perpendicular (y direction) diffusion coefficients of neutrally buoyant particles of different radii initially placed at various distances from the tube wall, in a quiescent medium. As mentioned earlier, in the diffusive regime, the

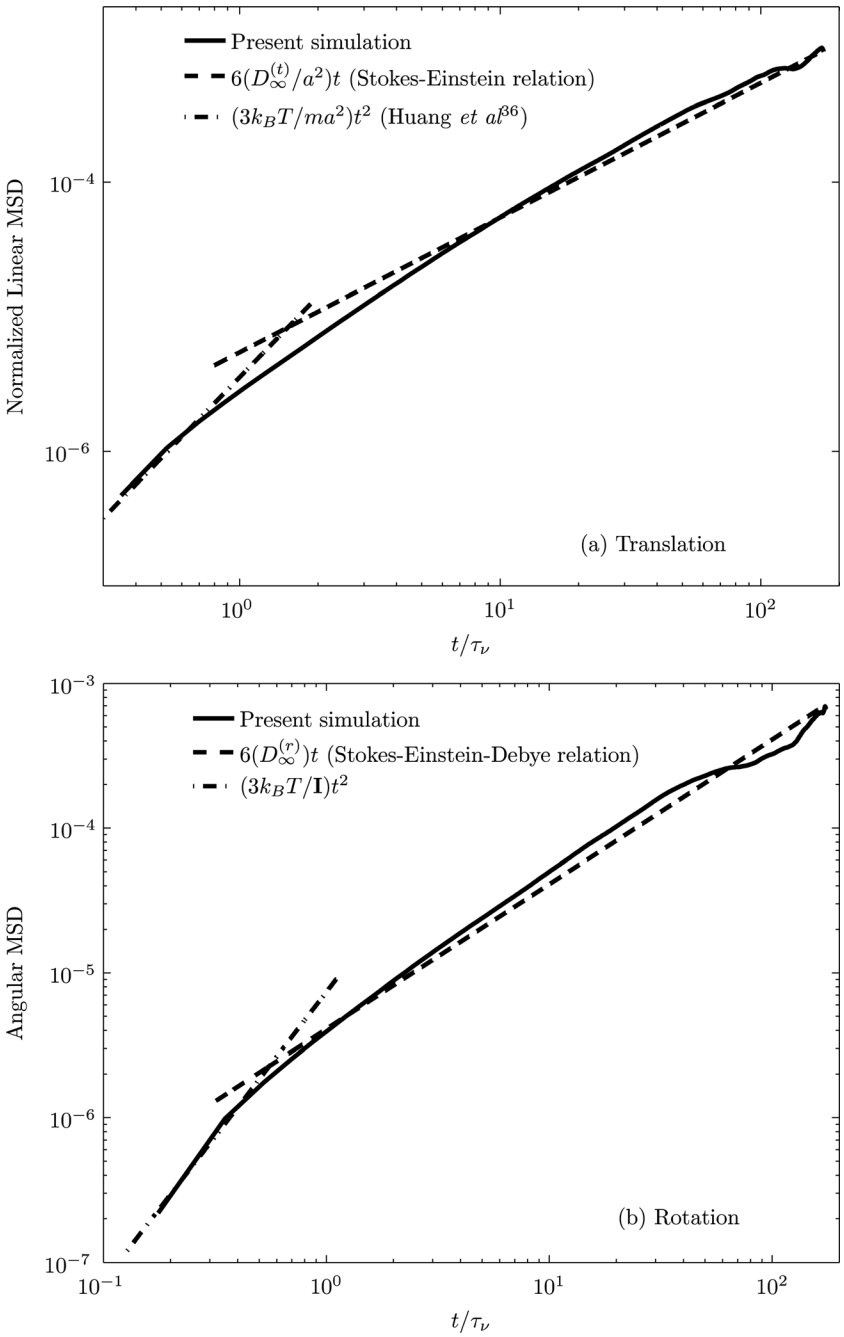

FIG. 11. The MSD of a neutrally buoyant Brownian particle ($a = 250\,\text{nm}$) in a stationary fluid medium using fluctuating hydrodynamics.

translational MSD of the particle increases linearly in time. We have numerically evaluated the gradient of the linear profile, normalized by the translational self-diffusion coefficient, $D_\infty^{(t)}$, plotted as a function of a/h. Our numerical results are in agreement with the predictions of Happel and Brenner.[55]

For the motion of a Brownian particle in shear flows, we have to consider an additional time scale $1/\dot{\gamma}$, where $\dot{\gamma}$ is the rate of shear. Where $\tau_b \ll t \ll 1/\dot{\gamma}$, the effect of convection due to the shear flow is weak. This is referred to as the diffusive regime for shear flows. The regime where $t \gg 1/\dot{\gamma}$ is dominated by convection. In this study, we have only explored the diffusive regime. In this regime, for the time scales considered, the MSDs in x, y, and z directions are all $\simeq 2D_\infty^{(t)}t$.[58,59]

We have numerically evaluated the diffusivity of a particle, $D_w^{(t)}$, initially located close to the wall in Poiseuille flow. The flow and particle Reynolds numbers are $Re_f = 0.005$ and $Re_p = 0.0025$, respectively. Figure 13 shows the parallel (x direction) and perpendicular (y direction) translational diffusion coefficients which have been normalized with $D_\infty^{(t)}$ as a function of a/h. These are for neutrally buoyant particles of different radii a initially placed at various locations h from the tube wall. There are analytical studies which predict the diffusivities, $D_w^{(t)}$, by perturbation theory.[55,57,60] Our numerical predictions show good comparison with the theoretical results. This capability of the simulation is particularly useful in the context of TDD.

Figure 14 demonstrates the approximate number of CPU cycles required for the computation of a single time step for a particle of radius 250 *nm* in a cylindrical tube of radius 5 μm. All simulations are carried out on a 2.93 GHz processor. Each CPU cycle displayed on the figure corresponds to

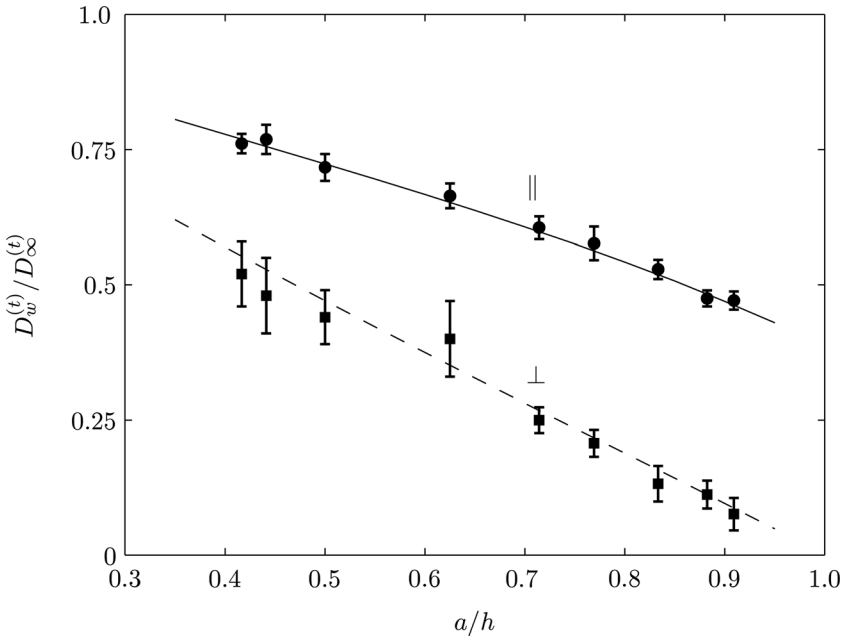

FIG. 12. The translational diffusion coefficient of neutrally buoyant Brownian particles of different radii a initially placed at different locations h from the wall of the circular vessel in a quiescent medium. Solid and dashed lines correspond to the perturbation solutions given in Happel and Brenner (Ref. 55).

the average of 300 time steps, spread across three realizations. The number of mesh nodes is displayed on the horizontal axis. Number of days required to complete the simulations with 20 000 time steps are specified inside the brackets and for 100 000 time steps this will be five times higher.

In regard to mesh nodes, we offer the following estimates from our numerical simulation corresponding to converged solutions. For a particle that is initially located at the center of the circular vessel in a quiescent medium, a small region ($1\,\mu\text{m}^3$ cube) around the particle ($a = 250\,\text{nm}$) is noted to have 34% of total number of mesh nodes in the entire volume, at convergence. For a particle initially located at a distance half way between the vessel center and the vessel wall ($h = R/2$), in an equivalent volume, we note there are 35% of total number of mesh nodes. Finally, when $h < R/2$, the estimate is 38%. These observations imply that for tracking a nanoparticle Brownian motion in a quiescent fluid, the mesh size has to be considerably smaller even at regions far away from the wall and would have to be finer in the vicinity of the wall. Our numerical simulation has handled these features in a comprehensive way yielding converged solutions to desired levels of accuracy ($\mathcal{O}(10^{-9})$).

V. CONCLUSIONS

A direct numerical simulation based on ALE FEM is employed to simulate the Brownian motion of a nanoparticle in an incompressible Newtonian fluid. Corrections for compressibility effects are introduced. The thermal force from the fluid is incorporated by the fluctuating hydrodynamics approach. Both the translational and rotational motions of a

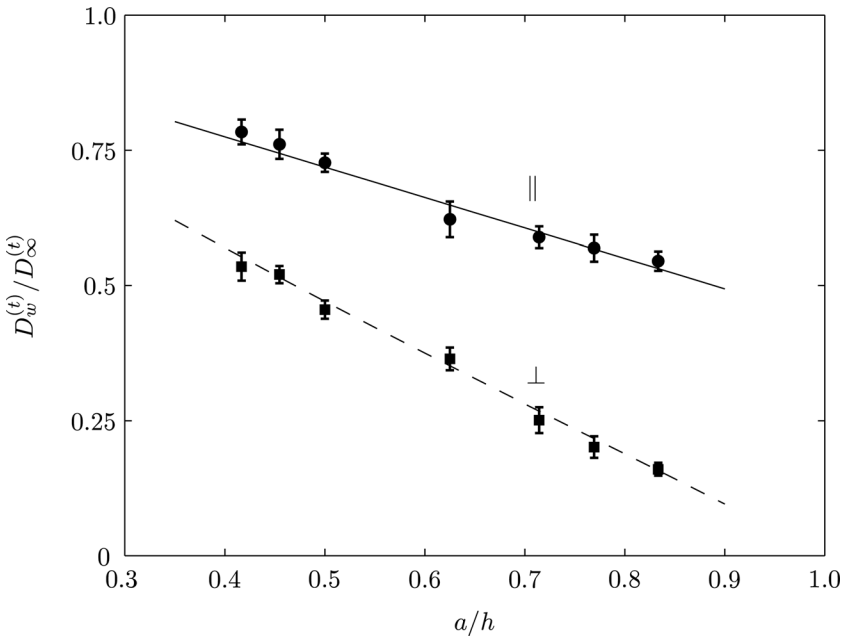

FIG. 13. The translational diffusion coefficient of neutrally buoyant Brownian particles of different radii a initially placed at different locations h from the wall of the circular tube in Poiseuille flow, in the diffusive regime $\tau_b \ll t \ll 1/\dot{\gamma}$. Solid and dashed lines correspond to the perturbation solutions given in Happel and Brenner (Ref. 55) and Goldman *et al.* (Ref. 60).

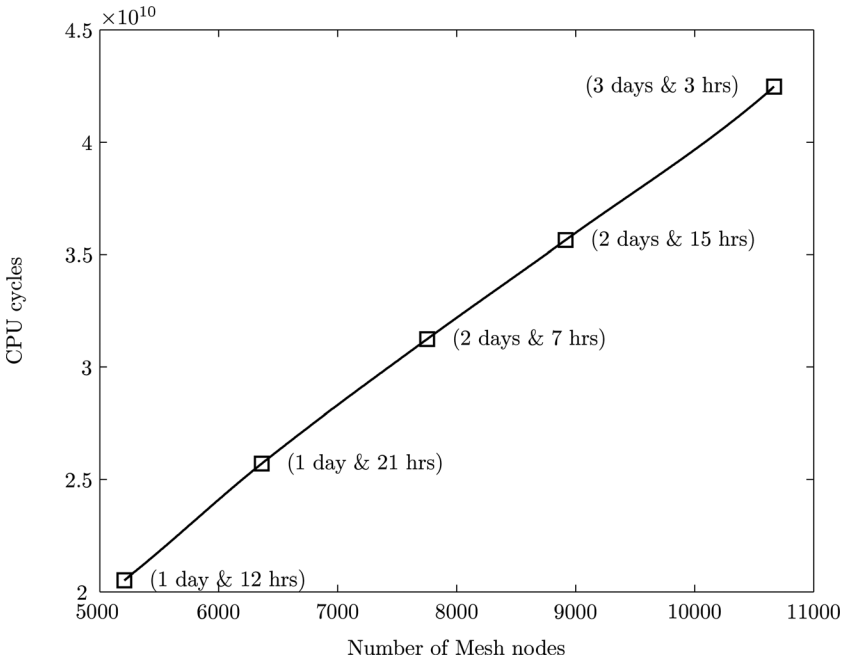

FIG. 14. Computational cost *for* fluctuating hydrodynamics. Number of days required to complete the simulations with 20 000 time steps are specified inside the brackets.

nanoparticle in (i) a quiescent fluid and (ii) a fully developed Poiseuille flow are considered. The thermal fluctuations are modeled as random stress tensors in the fluid equation that depend on the temperature and viscosity of the fluid. At thermal equilibrium, the numerical predictions are validated with analytical results, where available.

We have numerically predicted:

(a) The translational and rotational temperatures of the particle with and without bulk flow. The temperature calculation is carried out till thermal equilibration is obtained between the particle and the fluid medium. Both for quiescent and Poiseuille flow, in the range of fluid velocities considered, the equipartition theorem is satisfied.
(b) The translational and rotational temperatures of nearly neutrally buoyant Brownian particles, thermally equilibrated, in a quiescent fluid. These temperatures are noted to be independent of the density of the particle in relation to that of the fluid.
(c) The translational and rotational velocity distributions of the nanoparticle motion with and without bulk flow.
(d) The translational and rotational VACFs in a quiescent fluid. Over long times, the decay of the VACF captures algebraic tails for the translational ($t^{-3/2}$) and the rotational ($t^{-5/2}$) motions of the nanoparticle.
(e) The translational and rotational MSDs of the particle in a quiescent fluid, both for ballistic and diffusive regimes. At short times, translational and rotational MSDs in a quiescent fluid are proportional to t^2, and in the diffusive regime ($t \gg \tau_b$), they agree with the Stokes-Einstein and Stokes-Einstein-Debye theories.
(f) The effects of the presence of the bounding wall on particles of different radii initially placed at various locations are evaluated for several cases with and without bulk flow. The translational diffusion coefficients for parallel and perpendicular directions have been displayed. Very good agreement with published results, where available.

We have also provided the computational cost for fluctuating hydrodynamics.

In regard to biological applications intended in this study, it is noted that this method may be used to investigate the fluctuating motion of a nanocarrier in a particulate suspension where the dispersion in nanocarrier velocities are athermal in origin caused by collisions with red-blood cells. In such an application, the preset temperature must be replaced by a particulate temperature of blood plasma,[37] and this will form a part of our future work.

ACKNOWLEDGMENTS

This work was sponsored by National Institute of Health (NIH) Grant R01 EB006818 (DME); National Science Foundation (NSF) Grant CBET-0853389. Computational resources were provided in part by the National Partnership for Advanced Computational Infrastructure under Grant No. MCB060006.

[1]R. Kubo, "The fluctuation-dissipation theorem," Rep. Prog. Phys. **29**, 255 (1966).
[2]R. Kubo, M. Toda, and N. Hashitsume, *Nonequilibrium Statistical Mechanics*, 2nd ed., (Springer-Verlag, Berlin, 1991), Vol. II.
[3]P. Langevin, "On the theory of Brownian motion," C. R. Acad. Sci. **146**, 530 (1908).
[4]L. D. Landau and E. M. Lifshitz, *Fluid Mechanics* (Pergamon, London, 1959).
[5]M. Bixon and R. Zwanzig, "Boltzmann-Langevin equation and hydrodynamic fluctuations," Phys. Rev. **187**, 267 (1969).
[6]N. Sharma and N. A. Patankar, "Direct numerical simulation of the Brownian motion of particles by using fluctuating hydrodynamic equations," J. Comput. Phys. **201**, 466 (2004).
[7]A. Donev, E. Vanden-Eijnden, A. L. Garcia, and J. B. Bell, "On the accuracy of explicit finite-volume schemes for fluctuating hydrodynamics," Commun. Appl. Math. Comput. Sci. **5**, 149 (2010).
[8]A. J. C. Ladd, "Short-time motion of colloidal particles: Numerical simulation via a fluctuating lattice-Boltzmann equation," Phys. Rev. Lett. **70**, 1339 (1993).
[9]A. J. C. Ladd, "Numerical simulations of particulate suspensions via a discretized Boltzmann equation. Part 1. Theoretical foundation," J. Fluid Mech. **271**, 285 (1994).

[10]A. J. C. Ladd, "Numerical simulations of particulate suspensions via a discretized Boltzmann equation. Part 2. Numerical results," J. Fluid Mech., **271**, 311 (1994).
[11]N. A. Patankar, "Direct numerical simulation of moving charged, flexible bodies with thermal fluctuations," in *Technical Proceedings of the 2002 International Conference on Computational Nanoscience and Nanotechnology* (Nano Science and Technology Institute, 2002), Vol. 2, pp. 93–96.
[12]R. Adhikari, K. Stratford, M. E. Cates, and A. J. Wagner, "Fluctuating lattice Boltzmann," Euro Phys. Lett. **71**, 473 (2005).
[13]B. Dünweg and A. J. C. Ladd, "Lattice Boltzmann simulations of soft matter systems," Adv. Polym. Sci. **221**, 89 (2008).
[14]D. Nie and J. Lin, "A fluctuating lattice-Boltzmann model for direct numerical simulation of particle Brownian motion," Particuology **7**, 501 (2009).
[15]P. J. Atzberger, P. R. Kramer, and C. S. Peskin, "A stochastic immersed boundary method for fluid-structure dynamics at microscopic length scales," J. Comput. Phys. **224**, 1255 (2007).
[16]N. K. Voulgarakis and J. W. Chu, "Bridging fluctuating hydrodynamics and molecular dynamics simulations of fluids," J. Chem. Phys. **130**, 134111 (2009).
[17]N. K. Voulgarakis, S. Satish, and J. W. Chu, "Modeling the nanoscale viscoelasticity of fluids by bridging non-Markovian fluctuating hydrodynamics and molecular dynamics simulations," J. Chem. Phys. **131**, 234115 (2009).
[18]M. Serrano and P. Español, "Thermodynamically consistent mesoscopic fluid particle model," Phys. Rev. E **64**, 046115 (2001).
[19]M. Serrano, D. Gianni, P. Español, E. Flekkøy, and P. Coveney, "Mesoscopic dynamics of voronoi fluid particles," J. Phys. A **35**, 1605 (2002).
[20]M. Grmela and H. Öttinger, "Dynamics and thermodynamics of complex fluids. I. Development of a general formalism," Phys. Rev. E **56**, 6620 (1997).
[21]H. Öttinger and M. Grmela, "Dynamics and thermodynamics of complex fluids. II. Illustrations of a general formalism," Phys. Rev. E **56**, 6633 (1997).
[22]H. Hu, "Direct simulation of flows of solid-liquid mixtures," Int. J. Multiphase Flow **22**, 335 (1996).
[23]H. H. Hu, N. A. Patankar, and M. Y. Zhu, "Direct numerical simulations of fluid-solid systems using the arbitrary Langrangian-Eulerian technique," J. Comput. Phys. **169**, 427 (2001).
[24]L. Zhang, A. Gerstenberger, X. Wang, and W. K. Liu, "Immersed finite element method," Comput. Methods Appl. Mech. Eng. **193**, 2051 (2004).
[25]X. S. Wang, L. T. Zhang, and W. K. Liu, "On computational issues of immersed finite element methods," J. Comput. Phys. **228**, 2535 (2009).
[26]P. L. George, *Automatic Mesh Generation: Application to Finite Element Methods* (Wiley, New York, 1991).
[27]T. N. Swaminathan, K. Mukundakrishnan, and H. H. Hu, "Sedimentation of an ellipsoid inside an infinitely long tube at low and intermediate Reynolds numbers," J. Fluid Mech. **551**, 357 (2006).
[28]T. N. Swaminathan, H. H. Hu, and A. A. Patel, "Numerical analysis of the hemodynamics and embolus capture of a greenfield vena cava filter," J. Biomech. Eng. **128**, 360 (2006).
[29]K. Mukundakrishnan, H. H. Hu, and P. S. Ayyaswamy, "The dynamics of two spherical particles in a confined rotating flow: pedalling motion," J. Fluid Mech. **599**, 169 (2008).
[30]P. Español, J. Anero1, and I. Zúñiga, "Microscopic derivation of discrete hydrodynamics," J. Chem. Phys. **131**, 244117 (2009).
[31]J. Bell, A. Garcia, and S. Williams, "Numerical methods for the stochastic Landau-Lifshitz Navier-Stokes equations," Phys. Rev. E **76**, 016708 (2007).
[32]S. Williams, J. Bell, and A. Garcia, "Algorithm refinement for fluctuating hydrodynamics," Multiscale Model. Simul. **6**, 1256 (2008).
[33]R. Zwanzig and M. Bixon, "Hydrodynamic theory of the velocity correlation function," Phys. Rev. A **2**, 2005 (1970).
[34]R. Zwanzig and M. Bixon, "Compressibility effects in the hydrodynamic theory of Brownian motion," J. Fluid Mech. **69**, 21 (1975).
[35]T. Li, S. Kheifets, D. Medellin, and M. Raizen, "Measurement of the instantaneous velocity of a Brownian particle," Science **328**, 1673 (2010).
[36]R. Huang, I. Chavez, K. Taute, B. Lukic, S. Jeney, M. Raizen, and E. Florin, "Direct observation of the full transition from ballistic to diffusive Brownian motion in a liquid," Nature Phys. **7**, 576 (2011).
[37]L. L Munn, R. J. Melder, and R. K. Jain, "Role of erythrocytes in leukocyte-endothelial interactions: mathematical model and experimental validation," Biophys. J. **71**, 466 (1996).
[38]J. Liu, G. E. R. Weller, B. Zern, P. S. Ayyaswamy, D. M. Eckmann, V. R. Muzykantov, and R. Radhakrishnan, "A computational model for nanocarrier binding to endothelium validated using in vivo, in vitro, and atomic force microscopy experiments," Proc. Natl. Acad. Sci. U.S.A. **107**, 16530 (2010).
[39]K. Mukundakrishnan, S. Quan, D. M. Eckmann, and P. S. Ayyaswamy, "Numerical study of wall effects on buoyant gas-bubble rise in a liquid-filled finite cylinder," Phys. Rev. E **76**, 036308 (2007).
[40]K. Mukundakrishnan, P. S. Ayyaswamy, and D. M. Eckmann, "Finite-sized gas bubble motion in a blood vessel: non-newtonian effects," Phys. Rev. E **78**, 036303 (2008).
[41]S. Muro and V. R. Muzykantov, "Targeting of antioxidant and anti-thrombotic drugs to endothelial cell adhesion molecules," Curr. Pharm. Des. **11**, 2383 (2005).
[42]V. Muzykantov, "Biomedical aspects of targeted delivery of drugs to pulmonary endothelium," Expert Opin. Drug Delivery **2**, 909 (2005).
[43]B. S. Ding, T. Dziubla, V. V. Shuvaev, S. Muro, and V. R. Muzykantov, "Advanced drug delivery systems that target the vascular endothelium," Mol. Interv. **6**, 98 (2006).
[44]A. J. Calderon, V. Muzykantov, S. Muro, and D. M. Eckmann, "Flow dynamics, binding and detachment of spherical carriers targeted to icam-1 on endothelial cells," Biorheology **46**, 323 (2009).
[45]E. H. Hauge and A. Martin-Löf, "Fluctuating hydrodynamics and Brownian motion," J. Stat. Phys. **7**, 259 (1973).
[46]P. Español, M. Serrano, and H. Öttinger, "Thermodynamically admissible form for discrete hydrodynamics," Phys. Rev. Lett. **83**, 4542 (1999).
[47]T. J. R. Hughes, W. K. Liu, and T. K. Zimmermann, "Lagrangian-Eulerian finite element formulation for incompressible viscous flows," Comput. Methods Appl. Mech. Eng. **29**, 329 (1981).
[48]N. A. Patankar, P. Singh, D. D. Joseph, R. Glowinski, and T. W. Pan, "A new formulation of the distributed Lagrange multiplier/fictitious domain method for particulate flows," Int. J. Multiphase Flow **26**, 1509 (2000).
[49]Y. Chen, N. Sharma, and N. Patankar, "Fluctuating immersed material (fimat) dynamics for the direct numerical simulation of the Brownian motion of particles," in *Proceedings of the IUTAM Symposium on Computational Multiphase Flow*, edited by S. Balachandar and A. Prosperetti (Springer Verlag, 2006), pp. 119–129.
[50]P. Español and I. Zúñiga, "On the definition of discrete hydrodynamic variables," J. Chem. Phys. **131**, 164106 (2009).
[51]Y. Saad, *Iterative Methods for Sparse Linear Systems* (PWS Publ. Co., Boston, 1996).
[52]A. Einstein, "On the molecular-kinetic theory of the movement by heat of particles suspended in liquids at rest," Ann. Phys. **17**, 549 (1905).
[53]R. Zwanzig, *Nonequilibrium Statistical Mechanics* (Oxford University Press, New York, 2001).
[54]D. M. Heyes, M. J. Nuevo, J. J. Morales, and A. C. Branka, "Translational and rotational diffusion of model nanocolloidal dispersions studied by molecular dynamics simulations," J. Phys.: Condens. Matter **10**, 10159 (1998).
[55]J. Happel and H. Brenner, *Low Reynolds Number Hydrodynamics* (Martinus Nijhoff Publishers, Hague, 1983).
[56]G. Mavrovouniotis and H. Brenner, "Hindered sedimentation, diffusion, and dispersion coefficients for Brownian spheres in circular cylindrical pores," J. Colloid Interface Sci. **124**, 269 (1988).
[57]H. Brenner and L. Gaydos, "The constrained Brownian movement of spherical particles in cylindrical pores of comparable radius: Models of the diffusive and convective transport of solute molecules in membranes and porous media," J. Colloid Interface Sci. **58**, 312 (1977).
[58]M. San Miguel and J. Sancho, "Brownian motion in shear flow," Physica A-Stat. Mech. Appl. **99**, 357 (1979).
[59]R. T. Foister and T. G. M. V. D. Ven, "Diffusion of Brownian particles in shear flows," J. Fluid Mech. **96**, 105 (1980).
[60]A. J. Goldman, R. G. Cox, and H. Brenner, "Slow viscous motion of a sphere parallel to a plane wall—II Couette flow," Chem. Eng. Sci. **22**, 653 (1967).